OPTIMIZED JPEG IMAGE DECOMPRESSION WITH SUPER-RESOLUTION INTERPOLATION USING MULTI-ORDER TOTAL VARIATION

Shunsuke Ono and Isao Yamada

Department of Communications and Integrated Systems, Tokyo Institute of Technology,
Meguro-ku, Tokyo 152-8550, Japan

ABSTRACT

We propose a novel framework to obtain an artifact-free enlarged image from a given JPEG image. The proposed formulation based on a newly introduced JPEG image acquisition model realizes decompression and super-resolution interpolation simultaneously using multi-order total variation, so that we can drastically reduce artifacts appearing in JPEG images such as block noise and mosquito noise, without generating staircasing effect, which is typical in existing total variation-based JPEG decompression methods. We also present a computationally-efficient optimization scheme, derived as a special case of a primal-dual splitting type algorithm, for solving the convex optimization problem associated with the proposed formulation. Numerical examples show that the proposed method works effectively compared with existing methods.

***Index Terms*—** Convex optimization, multi-order total variation, optimized decompression, super-resolution interpolation

1. INTRODUCTION

JPEG is undoubtedly one of the most standard image compression techniques from more than twenty years ago to current. It is well-known that JPEG images often contain specific artifacts, such as block noise and mosquito noise, that severely degrade their perceptual quality. Motivated by the longstanding popularity of JPEG and the demand for the refinement of JPEG images whose original images are no longer available, the improvement of the JPEG decompression procedure has been widely studied (see [1, 2] for comprehensive review). One of the most effective approaches for this issue is to use the so-called *total variation* [3] (TV), as TV-based JPEG decompression methods having been developed [4, 5, 6]. In these methods, the JPEG decompression is modeled into a constrained minimization problem in which TV is minimized with constraint with respect to the quantization level of the blockwise DCT (discrete cosine transform) coefficients of a given JPEG image (we shall call it the *Q-constraint*). Suppressing TV well smoothes images, and the Q-constraint expresses a tight range containing the unknown original DCT coefficients, i.e., a resonable fidelity to the original image, so that the TV-based JPEG decompression methods can efficiently reduce the artifacts in JPEG images while keeping their original structure. Moreover, it does not require any complex and/or heuristic procedure, such as classification and segmentation, and the convexity of the objective function allows us to find a global solution (an artifact-free image) using computationally-efficient convex optimization algorithms.

However, it is known that the use of TV often results in an unfavorable *staircasing effect*, which indicates the need of a more suitable design of objective functions for the JPEG decompression. At the same time, in association with the spread of high-resolution devices, an efficient enlargement for a given JPEG image, which has not considered in existing TV-based JPEG decompression methods, has also been demanded.

With these in mind, we propose a method for obtaining an artifact-free enlarged image from a given JPEG image. The first contribution is to introduce a new JPEG image acquisition model including certain blurring (corresponds to a low-pass filter) and downsampling operations, which are determined based on the enlargement ratio, in order to consider the spatial regularity accompanied by enlargement. This model translates the problem of the JPEG decompression with super-resolution interpolation into an inverse problem, and it is rewritten as a convex optimization problem, that is, the minimization of multi-order TV with the Q-constraint. This problem formulation is the second contribution of this paper. Multi-order/higher order TV [7, 8, 9, 10, 11, 12] has mainly been introduced for image denoising, and it is known to be effective for reducing the staircasing effect. We specifically adopt the so-called *total generalized variation* [10, 11] (TGV) (Note: our framework can also employ other multi-order TVs). The third contribution is to present an optimization scheme, which is a special case of the primal-dual splitting algorithm [13], for efficiently solving the proposed convex optimization problem.

The rest of the paper is organized as follows. In the next section, we introduce minimal preliminaries necessary for the proposed method. Then, the proposed method is presented in Section 3. Corresponding numerical examples are shown in Section 4. Finally, we conclude the paper in Section 5.

2. PRELIMINARIES

In the following, $\mathbb{N}$, $\mathbb{R}$, $\mathbb{R}_+$, and $\mathbb{R}_{++}$ denote the sets of positive integers, all, nonnegative, and positive real numbers, respectively.

2.1. Standard JPEG compression and decompression

Let $\mathbf{\Psi} : \mathbb{R}^{m_v \times m_h} \rightarrow \mathbb{R}^{m_v \times m_h}$ ($m_v, m_h \in \mathbb{N}$) the blockwise DCT ($\mathbf{\Psi}^{-1}$ denotes its inverse) with the block size $b \times b$ (basically 8×8). Assume that m_v and m_h are divisible by b. In the standard JPEG compression procedure, first, an original image $\mathbf{U}_{\mathrm{org}} \in \mathbb{R}^{m_v \times m_h}$ is transformed into the blockwise DCT coefficients $\mathbf{\Theta}_{\mathbf{U}_{\mathrm{org}}} := \mathbf{\Psi}(\mathbf{U}_{\mathrm{org}}) \in \mathbb{R}^{m_v \times m_h}$. Second, these coefficients are quantized by a quantization table (Q-table) $\mathbf{Q} \in \mathbb{R}^{b \times b}$. Specifically, by letting $\mathbf{\Theta}^{(p)}_{\mathbf{U}_{\mathrm{org}}} \in \mathbb{R}^{b \times b}$ be the DCT coefficients of the p-th block of the original image, the quantized DCT coefficients of the block are given by $\mathcal{R}(\mathbf{\Theta}^{(p)}_{\mathbf{U}_{\mathrm{org}}}./\mathbf{Q})$, where $./$ denotes the element-wise division, and $\mathcal{R}$ the procedure rounding each element

This work is supported in part by JSPS Grants-in-Aid for JSPS fellows (24·2522) and (B-21300091).

to the nearest integer. Note that the Q-table $\mathbf{Q}$ is uniform to all blocks. Then, the quantized DCT coefficients and the Q-table are stored. The decompressed JPEG image $\mathbf{U}_{\text{jpg}} \in \mathbb{R}^{m_v \times m_h}$ is obtained by applying the blockwise inverse DCT to the dequantized DCT coefficients $\boldsymbol{\Theta}_{\mathbf{U}_{\text{jpg}}} \in \mathbb{R}^{m_v \times m_h}$, i.e., $\mathbf{U}_{\text{jpg}} = \boldsymbol{\Psi}^{-1}(\boldsymbol{\Theta}_{\mathbf{U}_{\text{jpg}}})$, where $\boldsymbol{\Theta}^{(p)}_{\mathbf{U}_{\text{jpg}}} = \mathcal{R}(\boldsymbol{\Theta}^{(p)}_{\mathbf{U}_{\text{org}}}./\mathbf{Q}).*\mathbf{Q}$ ($.*$ denotes the element-wise multiplication).

2.2. Total Generalized Varation

Let $\mathbf{D} \in \mathbb{R}^{n_v \times n_h}$ ($n_v, n_h \in \mathbb{N}$) be a base difference matrix:

$$\mathbf{D} := \begin{bmatrix} -1 & 1 & 0 & 0 & \cdots & 0 \\ 0 & -1 & 1 & 0 & \cdots & 0 \\ \vdots & & \ddots & \ddots & & \vdots \\ 0 & \cdots & 0 & -1 & 1 & 0 \\ 0 & \cdots & 0 & 0 & -1 & 1 \\ 0 & \cdots & 0 & 0 & 0 & 0 \end{bmatrix}.$$

Suppose that an image of size $n_v \times n_h$ is treated as an $N(= n_v n_h)$-dimensional vector whose entries correspond to the raster-scanned pixels. Then we can define the vertical and horizontal discrete difference operators for such an image respectively as $\mathbf{D}_v := \mathbf{I}_N \otimes \mathbf{D} \in \mathbb{R}^{N \times N}$ and $\mathbf{D}_v := \mathbf{D} \otimes \mathbf{I}_N \in \mathbb{R}^{N \times N}$, where $\mathbf{I}_N$ is the identity matrix of size $N \times N$, and $\otimes$ stands for Kronecker product. By letting $\mathbf{D}_1 := [\mathbf{D}_v^T\ \mathbf{D}_h^T]^T \in \mathbb{R}^{2N \times N}$ ($\cdot^T$ denotes the transposition) and

$$\mathbf{G}_1 := \begin{bmatrix} -\mathbf{D}_v^T & \mathbf{O} \\ -\mathbf{D}_h^T & -\mathbf{D}_v^T \\ \mathbf{O} & -\mathbf{D}_h^T \end{bmatrix} \in \mathbb{R}^{3N \times 2N},$$

the *total generalized variation* [10, 11] (TGV) of order 2 is given by

$$\|\cdot\|_{\text{TGV}}^{(\boldsymbol{\alpha})} : \mathbb{R}^N \to \mathbb{R}_+ : \mathbf{x} \mapsto \min_{\mathbf{D}_1\mathbf{x}=\mathbf{p}+\mathbf{q}} \{\alpha_1 \|\mathbf{p}\|_{1,2}^{(2N)} + \alpha_2 \|\mathbf{G}_1\mathbf{q}\|_{1,2}^{(3N)}\},$$

where $\|\cdot\|_{1,2}^{(KN)} : \mathbb{R}^{KN} \to \mathbb{R}_+ : \mathbf{x} \mapsto \sum_{i=1}^N \sqrt{\sum_{k=0}^{K-1} x_{i+kN}^2}$, and $\boldsymbol{\alpha} := [\alpha_1\ \alpha_2]^T \in \mathbb{R}^2_{++}$. We should remark that this primal definition of TGV is first introduced by Setzer *et al*. in [11]. The use of TGV is known as a reasonable approach for reducing the staircasing effect while keeping the effectiveness of TV.

2.3. Primal-Dual Splitting Algorithm

Let $\mathcal{H}$ be a real Hilbert space equipped with the standard inner product $\langle \cdot, \cdot \rangle$ and its induced norm $\|\cdot\|$. Consider the following convex optimization problem: find $\mathbf{x}^\star$ in

$$\arg\min_{\mathbf{x}\in\mathcal{H}} g(\mathbf{x}) + h(L\mathbf{x}), \tag{1}$$

where $g \in \Gamma_0(\mathcal{H})$[1], $h \in \Gamma_0(\mathcal{K})$ ($\mathcal{K}$ is another real Hilbert space), and $L : \mathcal{H} \to \mathcal{K}$ a bounded linear operator. Then the primal-dual splitting algorithm [13][2] for solving (1) is given as follows:

$$\left\lfloor \begin{array}{l} \mathbf{x}_{k+1} := \text{prox}_{\gamma_1 g}[\mathbf{x}_k - \gamma_1 L^* \boldsymbol{\xi}_k], \\ \boldsymbol{\xi}_{k+1} := \text{prox}_{\gamma_2 h^*}[\boldsymbol{\xi}_k + \gamma_2 L(2\mathbf{x}_{k+1} - \mathbf{x}_k)], \end{array} \right. \tag{2}$$

[1]A function $f : \mathcal{H} \to (-\infty, \infty]$ is called *proper lower semicontinuous convex* if $\text{dom}f := \{\mathbf{x} \in \mathcal{H} |\ f(\mathbf{x}) < \infty\} \neq \emptyset$, $\text{lev}_{\leq\alpha}(f) := \{\mathbf{x} \in \mathcal{H} |\ f(\mathbf{x}) \leq \alpha\}$ is closed for every $\alpha \in \mathbb{R}$, and $f(\lambda\mathbf{x} + (1-\lambda)\mathbf{y}) \leq \lambda f(\mathbf{x}) + (1-\lambda) f(\mathbf{y})$ for every $\mathbf{x}, \mathbf{y} \in \mathcal{H}$ and $\lambda \in (0, 1)$, respectively. The set of all proper lower semicontinuous convex functions over $\mathcal{H}$ is denoted by $\Gamma_0(\mathcal{H})$.

[2]It can solve a more general problem (see [13]).

where prox denotes the *proximity operator* [14] which is defined, for a function $J \in \Gamma_0(\mathcal{H})$ and an index $\gamma \in (0, \infty)$, by

$$\text{prox}_{\gamma J}(\mathbf{x}) := \arg\min_{\mathbf{y}\in\mathcal{H}} J(\mathbf{y}) + \tfrac{1}{2\gamma}\|\mathbf{x} - \mathbf{y}\|^2,$$

h^* the *Fenchel-Rockafellar conjugate function*[3] of h, L^* the adjoint operator of L, $\gamma_1, \gamma_2 \in \mathbb{R}_{++}$ satisfying $\gamma_1^{-1} - \gamma_2 \|L\|_{op}^2 > 0$ ($\|\cdot\|_{op}$ stands for the operator norm). Under some mild conditions, the sequence $(\mathbf{x}_k)_{k\in\mathbb{N}}$ converges (weakly) to $\mathbf{x}^\star$ in (1).

3. PROPOSED METHOD

3.1. Problem Formulation

Let $\overline{\mathbf{u}} \in \mathbb{R}^N$ be an unknown ideal enlarged image of size $n_v \times n_h (= N)$ we wish to obtain, and $\mathbf{v} \in \mathbb{R}^M$ ($M \leq N$) a given JPEG image of size $m_v \times m_h (= M)$. We first propose the following JPEG image acquisition model:

$$\mathbf{v} = \boldsymbol{\Psi}^{-1}\mathcal{Q}(\boldsymbol{\Psi}\mathbf{S}\mathbf{B}\mathbf{u}), \tag{3}$$

where $\mathcal{Q} : \mathbb{R}^M \to \mathbb{R}^M$ is a procedure performing quantization and dequantization, $\mathbf{S} \in \mathbb{R}^{M \times N}$ a linear downsampling operator, and $\mathbf{B} \in \mathbb{R}^{N \times N}$ a linear blurring operator. This model expresses JPEG compression and scale-down processes, so that we can translate the JPEG decompression with super-resolution interpolation into an inverse problem regarding the model.

Based on (3), we formulate a convex optimization problem to estimate $\overline{\mathbf{u}}$ from $\mathbf{v}$ as follows: find $\mathbf{u}^\star$ in

$$\arg \min_{\substack{\mathbf{u}\in C_{255} \\ \mathbf{S}\mathbf{B}\mathbf{u}\in C_{\mathbf{v}}^{\mathbf{Q}}}} \|\mathbf{u}\|_{\text{TGV}}^{(\boldsymbol{\alpha})}, \tag{4}$$

where the set C_{255} is defined by

$$C_{255} := \{\mathbf{x} \in \mathbb{R}^N |\ x_i \in [0, 255]\ \ (i = 1, \ldots, N)\},$$

which is a constraint on the intensity range of pixels in the case of 8-bit grayscale images, and the set $C_{\mathbf{v}}^{\mathbf{Q}}$ is defined by

$$C_{\mathbf{v}}^{\mathbf{Q}} := \{\mathbf{x} \in \mathbb{R}^M |\ \mathcal{R}(\boldsymbol{\Theta}_{\mathbf{x}}^{(p)}./\mathbf{Q}) = \mathcal{R}(\boldsymbol{\Theta}_{\mathbf{v}}^{(p)}./\mathbf{Q})\ \ (p = 1, \ldots, M/b^2)\},$$

where $\boldsymbol{\Theta}_{\mathbf{x}}^{(p)}$ and $\boldsymbol{\Theta}_{\mathbf{v}}^{(p)}$ respectively denote the DCT coefficients of the p-th block of $\mathbf{x}$ and $\mathbf{v}$ (where they are seen to be the original matrix forms). The set $C_{\mathbf{v}}^{\mathbf{Q}}$, which is what we call Q-constraint, represents a reasonably-tight range of each DCT coefficient, which we can know a priori. Meanwhile, the TGV in (4) plays the role to remove the block noise and mosquito noise in the resulting enlarged image, as well it can prevent the staircasing effect. Hence, by solving (4), we can expect to obtain an artifact-free enlarged image as $\mathbf{u}^\star$.

3.2. Optimization

In what follows, we reformulate (4) in order to solve it by (2). First, we give an equivalent expression of (4) as follows: find $\mathbf{u}^\star$ in

$$\arg\min_{\mathbf{u}\in\mathbb{R}^N} \min_{\mathbf{D}_1\mathbf{u}=\mathbf{p}+\mathbf{q}} \{\alpha_1\|\mathbf{p}\|_{1,2}^{(2N)} + \alpha_2\|\mathbf{G}_1\mathbf{q}\|_{1,2}^{(3N)}\} + \iota_{C_{255}}(\mathbf{u}) + \iota_{C_{\mathbf{v}}^{\mathbf{Q}}}(\mathbf{S}\mathbf{B}\mathbf{u}), \tag{5}$$

[3]The *Fenchel-Rockafellar conjugate function* of $f \in \Gamma_0(\mathcal{H})$ is defined by $f^*(\boldsymbol{\xi}) := \sup_{\mathbf{x}\in\mathcal{H}}\{\langle \mathbf{x}, \boldsymbol{\xi}\rangle - f(\mathbf{x})\}$. The proximity operator of f^* can be expressed as $\text{prox}_{\gamma f^*}(\mathbf{x}) = \mathbf{x} - \gamma\text{prox}_{\gamma^{-1}f}(\gamma^{-1}\mathbf{x})$.

where $\iota_{C_{255}}$ and $\iota_{C_{\mathbf{v}}^{\mathbf{Q}}}$ denote the indicator functions of the corresponding sets. The indicator function of a nonempty closed convex set $C \subset \mathcal{H}$ is defined by

$$\iota_C : \mathcal{H} \to \{0, \infty\} : \mathbf{x} \mapsto \begin{cases} 0, & \text{if } \mathbf{x} \in C, \\ \infty, & \text{otherwise.} \end{cases}$$

Second, using the equation $\mathbf{p} = \mathbf{D}_1\mathbf{u} - \mathbf{q}$, (5) can be rewritten as

$$\underset{\mathbf{r}\in\mathbb{R}^{3N}}{\arg\min}\ \alpha_1\|\mathbf{D}_1\mathbf{u} - \mathbf{q}\|_{1,2}^{(2N)} + \alpha_2\|\mathbf{G}_1\mathbf{q}\|_{1,2}^{(3N)} + \iota_{C_{255}}(\mathbf{u}) + \iota_{C_{\mathbf{v}}^{\mathbf{Q}}}(\mathbf{SBu}),$$

where $\mathbf{r} := [\mathbf{u}^T \mathbf{q}^T]^T$. Third, define a finite dimensional real Hilbert space $\mathcal{X} := \mathbb{R}^{2N} \times \mathbb{R}^{3N} \times \mathbb{R}^M$ equipped with the inner product $\langle\cdot,\cdot\rangle_{\mathcal{X}} := \langle\cdot,\cdot\rangle_{\mathbb{R}^{2N}} + \langle\cdot,\cdot\rangle_{\mathbb{R}^{3N}} + \langle\cdot,\cdot\rangle_{\mathbb{R}^M}$ and its induced norm, and

$$g : \mathbb{R}^{3N} \to \{0, \infty\} : \mathbf{r} \mapsto \iota_{C_{255}}(\mathbf{u}),$$
$$L : \mathbb{R}^{3N} \to \mathcal{X} : \mathbf{r} \mapsto (\mathbf{D}_1\mathbf{u} - \mathbf{q}, \mathbf{G}_1\mathbf{q}, \mathbf{SBu}),$$
$$h : \mathcal{X} \to [0, \infty] : (\mathbf{z}_1, \mathbf{z}_2, \mathbf{z}_3) \mapsto \alpha_1\|\mathbf{z}_1\|_{1,2}^{(2N)} + \alpha_2\|\mathbf{z}_2\|_{1,2}^{(3N)} + \iota_{C_{\mathbf{v}}^{\mathbf{Q}}}(\mathbf{z}_3).$$

Then (5) can be seen as a special case of (1), so that we can apply (2) to it. As a result, we obtain an algorithmic solution to (4) as shown in Algorithm 3.1, which does not require a matrix inversion and/or other complicated procedures. The sequence $(\mathbf{u}^{(n)})_{n\in\mathbb{N}}$ in Algorithm 3.1 converges to $\mathbf{u}^\star$ in (4). The detailed explanation of the implementation of Algorithm 3.1 is summarized in Remark 3.1.

Algorithm 3.1 Solver for (4)

1: Set $n = 0$, and choose $\mathbf{u}^{(0)}, \mathbf{q}^{(0)}, \gamma_1, \gamma_2$.
2: $\mathbf{z}_1^{(0)} = \mathbf{D}_1\mathbf{u}^{(0)}, \mathbf{z}_2^{(0)} = \mathbf{G}_1\mathbf{q}^{(0)}, \mathbf{z}_3^{(0)} = \mathbf{SBu}^{(0)}$
3: **while** a stop criterion is not satisfied **do**
4: $\quad\mathbf{u}^{(n+1)} = \mathrm{prox}_{\gamma_1\iota_{C_{255}}}(\mathbf{u}^{(n)} - \gamma_1(\mathbf{D}_1^T\mathbf{z}_1^{(n)} + \mathbf{G}_1^T\mathbf{z}_2^{(n)} + \mathbf{B}^T\mathbf{S}^T\mathbf{z}_3^{(n)}))$
5: $\quad\mathbf{w}_1^{(n)} = \mathbf{z}_1^{(n)} + \gamma_2\mathbf{D}_1(2\mathbf{u}^{(n+1)} - \mathbf{u}^{(n)})$
6: $\quad\mathbf{w}_2^{(n)} = \mathbf{z}_2^{(n)} + \gamma_2\mathbf{G}_1(2\mathbf{u}^{(n+1)} - \mathbf{u}^{(n)})$
7: $\quad\mathbf{w}_3^{(n)} = \mathbf{z}_3^{(n)} + \gamma_2\mathbf{SB}(2\mathbf{u}^{(n+1)} - \mathbf{u}^{(n)})$
8: $\quad\hat{\mathbf{w}}_1^{(n)} = \mathrm{prox}_{\frac{\alpha_1}{\gamma_2}\|\cdot\|_{1,2}^{(2N)}}(\frac{1}{\gamma_2}\mathbf{w}_1^{(n)})$
9: $\quad\hat{\mathbf{w}}_2^{(n)} = \mathrm{prox}_{\frac{\alpha_2}{\gamma_2}\|\cdot\|_{1,2}^{(3N)}}(\frac{1}{\gamma_2}\mathbf{w}_2^{(n)})$
10: $\quad\hat{\mathbf{w}}_3^{(n)} = \mathrm{prox}_{\frac{1}{\gamma_2}\iota_{C_{\mathbf{v}}^{\mathbf{Q}}}}(\frac{1}{\gamma_2}\mathbf{w}_3^{(n)})$
11: $\quad\mathbf{z}_1^{(n+1)} = \mathbf{w}_1^{(n)} - \gamma_2\hat{\mathbf{w}}_1^{(n)}$
12: $\quad\mathbf{z}_2^{(n+1)} = \mathbf{w}_2^{(n)} - \gamma_2\hat{\mathbf{w}}_2^{(n)}$
13: $\quad\mathbf{z}_3^{(n+1)} = \mathbf{w}_3^{(n)} - \gamma_2\hat{\mathbf{w}}_3^{(n)}$
14: $\quad n = n + 1$
15: **end while**
16: Output $\mathbf{u}^{(n)}$

Remark 3.1 (Implementation of Algorithm 3.1)**.**

- $\mathrm{prox}_{\gamma\|\cdot\|_{1,2}^{(KN)}}$ in line 8 and 9: The proximity operator can be derived based on Proposition 2.8 of [15], which is given by

$$\mathrm{prox}_{\gamma\|\cdot\|_{1,2}^{(KN)}}(\mathbf{x}) = \mathrm{diag}(\underbrace{d_1, \dots, d_N, d_1, \dots\ \dots, d_N}_{KN})\mathbf{x},$$

  where $d_i := \max\{1 - \frac{\gamma}{\sqrt{\sum_{k=0}^{K-1} x_{i+kN}^2}}, 0\}$ for $i = 1, \dots, N$.
- $\mathrm{prox}_{\gamma\iota_{C_{255}}}$ in line 4: The proximity operator is equal to the metric projection onto C_{255} given by $P_{C_{255}}(\mathbf{x}) = \hat{\mathbf{x}}$, where $\hat{x}_i = 0$ if $x_i < 0$, $\hat{x}_i = 255$ if $x_i > 255$, $\hat{x}_i = x_i$ otherwise $(i = 1, \dots, N)$.
- $\mathrm{prox}_{\gamma\iota_{C_{\mathbf{v}}^{\mathbf{Q}}}}$ in line 10: The proximity operator is the metric projection onto $C_{\mathbf{v}}^{\mathbf{Q}}$ given by $P_{C_{\mathbf{v}}^{\mathbf{Q}}}(\mathbf{x}) = \mathbf{\Psi}^{-1}\widetilde{\mathbf{\Theta}}_{\mathbf{x}}$, where the (i,j)-th entry $(i, j = 1, \dots, b)$ of the p-th block $(p = 1, \dots, \frac{M}{b^2})$ of $\widetilde{\mathbf{\Theta}}_{\mathbf{x}}$, which we denote by $(\widetilde{\mathbf{\Theta}}_{\mathbf{x}}^{(p)})_{i,j}$ (likewise $(\mathbf{\Theta}_{\mathbf{x}}^{(p)})_{i,j}$ and $(\mathbf{\Theta}_{\mathbf{v}}^{(p)})_{i,j}$), is given by

$$(\widetilde{\mathbf{\Theta}}_{\mathbf{x}}^{(p)})_{i,j} := \begin{cases} (\mathbf{\Theta}_{\mathbf{x}}^{(p)})_{i,j}, & \text{if } \mathcal{R}((\mathbf{\Theta}_{\mathbf{x}}^{(p)})_{i,j}/Q_{i,j}) = T_{i,j}^{(p)}, \\ (\mathbf{\Theta}_{\mathbf{v}}^{(p)})_{i,j} - 0.5Q_{i,j}, & \text{if } \mathcal{R}((\mathbf{\Theta}_{\mathbf{x}}^{(p)})_{i,j}/Q_{i,j}) < T_{i,j}^{(p)}, \\ (\mathbf{\Theta}_{\mathbf{v}}^{(p)})_{i,j} + 0.5Q_{i,j}, & \text{if } \mathcal{R}((\mathbf{\Theta}_{\mathbf{x}}^{(p)})_{i,j}/Q_{i,j}) > T_{i,j}^{(p)}, \end{cases}$$

  $T_{i,j}^{(p)} := \mathcal{R}((\mathbf{\Theta}_{\mathbf{v}}^{(p)})_{i,j}/Q_{i,j})$, and $Q_{i,j}$ the (i,j)-th entry of the Q-table $\mathbf{Q}$.

4. NUMERICAL EXAMPLE

We examine the performance of the propose method using test JPEG images, which are generated as follows: the original standard images (256×256) are blurred by the 2×2 uniform blur kernel, downsampled to their half size (128×128), and then compressed by JPEG with the quality factor 30 (Figure 1(a1)-(a4)). We try to estimate the original 256×256 images (ideal enlarged images) from the generated JPEG 128×128 images. The proposed method is compared with the following two methods. The first method simply enlarges given JPEG images by the bicubic interpolation. The second method performs an optimized decompression by solving the following problem using the primal-dual splitting algorithm: find $\mathbf{u}^\star$ in

$$\underset{\substack{\mathbf{u}\in C_{255} \\ \mathbf{SBu}\in C_{\mathbf{v}}^{\mathbf{Q}}}}{\arg\min}\ \|\mathbf{u}\|_{\mathrm{TV}} := \|\mathbf{D}_1\mathbf{u}\|_{1,2}^{(2N)}, \tag{6}$$

which utilizes the standard TV and corresponds to the existing TV-based JPEG decompression model [6] with super-resolution interpolation (it is also a special case of (4)). Remark again that enlargement/super-resolution interpolation is not considered in [6]. This is to verify the effectiveness of the multi-order TV (TGV). In (4), we choose $\boldsymbol{\alpha} = [0.35\ 0.65]$ which gives the best performance on average in terms of SSIM [16]. The parameters and iteration number of Algorithm 3.1 are set as $(\gamma_1, \gamma_2) = (0.01, 10)$ and 1000. Those of the primal-dual algorithm for (6) are the same.

Resulting images are depicted in Figure 1. Fig. 1(b1)-(b4) are enlarged images by the first method (bicubic) where block noise and mosquito noise are severe. In Fig. 1(c1)-(c4), which are obtained by the second method (solving (6)), we observe considerable staircasing effect. On the other hand, such an effect does not occur in the resulting images of the proposed method as shown in Fig. 1(d1)-(d4). Moreover, the artifacts of JPEG are significantly removed, and their SSIM [16] are higher than the others, as well as better in terms of human eye perception.

5. CONCLUDING REMARKS

We have proposed a convex optimization-based JPEG image decompression with super-resolution interpolation. The proposed formulation employs multi-order TV (TGV) for removing typical artifacts in JPEG, and incorporates blurring and downsampling operators to take super-resolution interpolation into account, so that we can realize artifact-free decompression and enlargement simultaneously only by solving one convex optimization problem. Numerical examples illustrate that the proposed method restores artifact-free enlarged images without generating the staircasing effect.

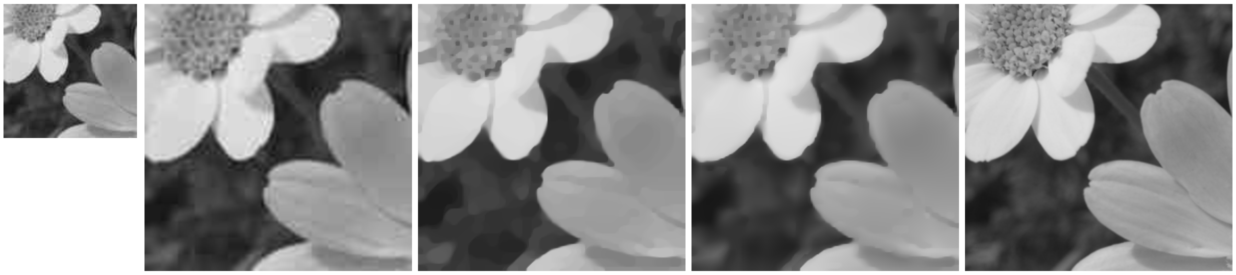

(a1) JPEG. (b1) Bicubic. PSNR = 31.48[dB] SSIM = 0.8846 (c1) Existing [6] with interpolation. PSNR = 31.50[dB] SSIM = 0.9002 (d1) Proposed. PSNR = 31.71[dB] SSIM = 0.9106 (e1) Oracle.

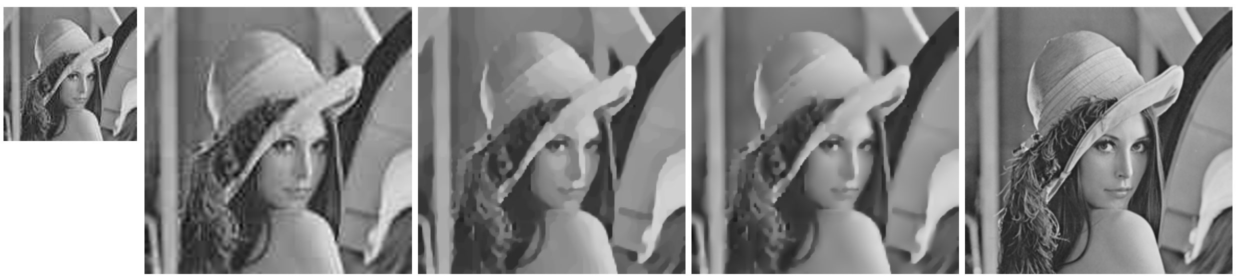

(a2) JPEG. (b2) Bicubic. PSNR = 26.78[dB] SSIM = 0.7830 (c2) Existing [6] with interpolation. PSNR = 26.44[dB] SSIM = 0.7780 (d2) Proposed. PSNR = 26.66[dB] SSIM = 0.7934 (e2) Oracle.

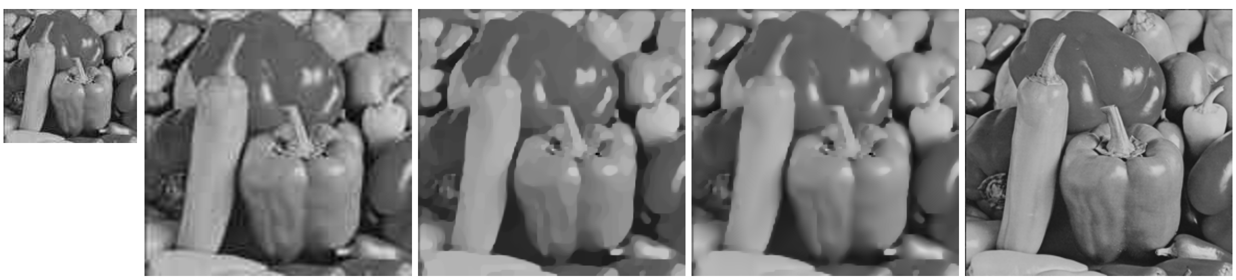

(a3) JPEG. (b3) Bicubic. PSNR = 27.33[dB] SSIM = 0.8213 (c3) Existing [6] with interpolation. PSNR = 26.73[dB] SSIM = 0.8286 (d3) Proposed. PSNR = 27.02[dB] SSIM = 0.8444 (e3) Oracle.

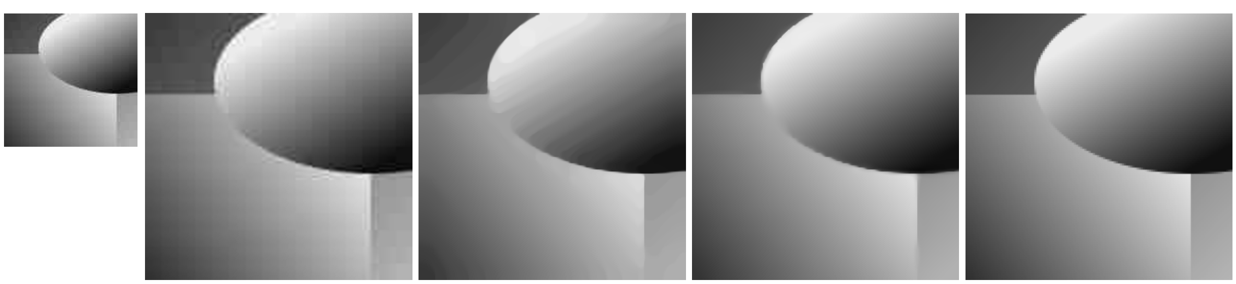

(a4) JPEG. (b4) Bicubic. PSNR = 37.38[dB] SSIM = 0.9648 (c4) Existing [6] with interpolation. PSNR = 39.08[dB] SSIM = 0.9865 (d4) Proposed. PSNR = 40.70[dB] SSIM = 0.9910 (e4) Oracle.

Fig. 1. *JPEG decompression with super-resolution interpolation results.*

We finally remark that the proposed method can employ other functions, e.g., the ℓ^1 norm of suitable frames and the block nuclear norm [17], in the combination with multi-order TV via hybrid regularization approaches [18, 19, 20], which may improve the performance. Future work includes an extension to color JPEG image case using functions for color image recovery, such as [21, 22, 23].

6. REFERENCES

[1] M.-Y. Shen and C.-C. Jay Kuo, "Review of postprocessing techniques for compression artifact removal," *J. Vis. Commun. and Image Represent.*, vol. 9, pp. 2–14, 1998.

[2] S. Singh, V. Kumar, and H. K. Verma, "Reduction of blocking artifacts in JPEG compressed images," *Digital Signal Processing*, vol. 17, pp. 225–243, 2007.

[3] L. I. Rudin, S. Osher, and E. Fatemi, "Nonlinear total variation based noise removal algorithms," *Phys. D*, vol. 60, no. 1-4, pp. 259–268, 1992.

[4] S. Zhong, "Image coding with optimal reconstruction," in *Proc. of IEEE ICIP*, 1997, pp. 161–164.

[5] F. Alter, S. Durand, and J. Froment, "Adapted total variation for artifact free decompression of jpeg images," *J. Math. Imag. Vis.*, vol. 23, pp. 199–211, 2005.

[6] K. Bredies and M. Holler, "A total variation-based JPEG decompression model," *SIAM J. Imaging Sci.*, vol. 5, no. 1, pp. 366–393, 2012.

[7] A. Chambolle and P. Lions, "Image recovery via total variation minimization and related problems," *Numerische Mathematik*, vol. 76, no. 2, pp. 167–188, 1997.

[8] M. Lysaker, "Iterative image restoration combining total variation minimization and a second order functional," *Int. J. Comput. Vis.*, vol. 66, no. 1, pp. 5–18, 2006.

[9] T. F. Chan, S. Esedoglu, and F. E. Park, "A fourth order dual method for staircase reduction in texture extraction and image restoration problems," in *Proc. of IEEE ICIP*, 2010, pp. 4137–4140.

[10] K. Bredies, K. Kunisch, and T. Pock, "Total generalized variation," *SIAM J. Imaging Sci.*, vol. 3, no. 3, pp. 92–526, 2010.

[11] S. Setzer, G. Steidl, and T. Teuber, "Infimal convolution regularizations with discrete ℓ_1-type functionals," *Communications in Mathematical Sciences*, vol. 9, no. 3, pp. 797–827, 2011.

[12] Y. Hu and M. Jacob, "Higher degree total variation (HDTV) regularization for image recovery," *IEEE Trans. Image Process.*, vol. 21, no. 5, pp. 2559–2571, 2012.

[13] L. Condat, "A primal-dual splitting method for convex optimization involving Lipschitzian, proximable and linear composite terms," *J. Optimization Theory and Applications*, 2013.

[14] J. J. Moreau, "Fonctions convexes duales et points proximaux dans un espace hilbertien," *C. R. Acad. Sci. Paris Ser. A Math.*, vol. 255, pp. 2897–2899, 1962.

[15] P. L. Combettes and J. C. Pesquet, "A proximal decomposition method for solving convex variational inverse problems," *Inverse Problems*, vol. 24, no. 6, 2008.

[16] Z. Wang, A. C. Bovik, H. R. Sheikh, and E. P. Simoncelli, "Image quality assessment: from error visibility to structural similarity," *IEEE Trans. Image Process.*, vol. 13, no. 4, pp. 600–612, 2004.

[17] S. Ono, T. Miyata, I. Yamada, and K. Yamaoka, "Missing region recovery by promoting blockwise low-rankness," in *Proc. of IEEE ICASSP*, 2012, pp. 1281–1284.

[18] N. Pustelnik, C. Chaux, and J.-C. Pesquet, "Parallel proximal algorithm for image restoration using hybrid regularization," *IEEE Trans. Image Process.*, vol. 20, no. 9, pp. 2450–2462, 2011.

[19] S. Ono, T. Miyata, and K. Yamaoka, "Total variation-wavelet-curvelet regularized optimization for image restoration," in *Proc. of IEEE ICIP*, 2011, pp. 2721–2724.

[20] S. Ono, T. Miyata, I. Yamada, and K. Yamaoka, "Image recovery by decomposition with component-wise regularization," *IEICE Trans. Fundamentals.*, vol. E95-A, no. 12, 2012.

[21] X. Bresson and T. F. Chan, "Fast dual minimization of the vectorial total variation norm and applications to color image processing," *Inverse Probl. Imag.*, vol. 2, no. 4, pp. 455–484, 2008.

[22] S. Ono and I. Yamada, "A convex regularizer for reducing color artifact in color image recovery," in *Proc. of CVPR*, 2013.

[23] T. Miyata, "L infinity total generalized variation for color image recovery," in *Proc. of IEEE ICIP*, 2013.